ACS Energy LETTERS

http://pubs.acs.org/journal/aelccp

Catalytic Proton–Hydroxide Recombination for Forward-Bias Bipolar Membranes

James B. Mitchell, Lihaokun Chen, Kurt Langworthy, Kevin Fabrizio, and Shannon W. Boettcher*

Cite This: *ACS Energy Lett.* 2022, 7, 3967–3973

Read Online

ACCESS | Metrics & More | Article Recommendations | Supporting Information

ABSTRACT: Bipolar membranes (BPMs) can generate steady-state pH gradients in electrochemical cells, enabling half-reactions to occur in different pH environments, and are thus of broad interest. Forward-bias BPMs further enable new approaches to fuel cells, redox-flow batteries, and CO_2 electrolyzers. In forward bias, the gradient in electrochemical potential drives ionic charge carriers toward the bipolar junction where they can recombine. We use a H_2-pump electrochemical cell to study H^+/OH^- recombination at the bipolar junction. We discover that metal-oxide nanoparticles catalyze the recombination reaction in the bipolar junction under forward bias and find evidence that H^+/OH^- recombination occurs via a surface mechanism on the oxide catalyst. We propose a rate equation to describe the catalytic H^+/OH^- recombination mechanism, supported by numerical simulations. This work thus elucidates materials-design strategies for recombination catalysts to advance forward-bias BPM technologies.

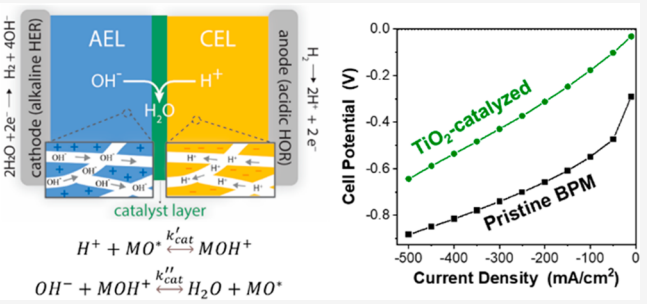

Bipolar membranes (BPMs) consist of two oppositely charged, polymeric, ion-exchange layers—cation- and anion-exchange layers (CEL and AEL, respectively)—laminated together to form a bipolar junction.[1−3] BPMs are used commercially in electrodialysis (BPMED), where the BPM is combined in a flow cell with anion- and cation-selective membranes to generate acid and base from brine solutions for wastewater management.[1,4−6] BPMs could also advance electrochemical technologies, such as water and CO_2 electrolyzers,[7−11] due to the capability to support pH gradients and thus enable two electrochemical half-reactions to occur in different pH environments.[3] BPMs thus allow for coupling acidic and alkaline half-reactions previously unrealizable in conventional membrane-based electrochemical technologies.[3]

Most applications use BPMs in reverse-bias mode. One example is in a bipolar-membrane-electrode assembly (BPMEA) with an acidic cathode and a basic anode (Figure 1a).[12] When sufficient reverse bias is applied, water dissociation (WD; $H_2O \rightarrow H^+ + OH^-$) is driven at the bipolar junction to form OH^- and H^+, which are moved out of the BPM in opposite directions by the electrochemical potential gradient.[13] In forward-bias mode (Figure 1b), however, the anode is acidic and the cathode basic; ions are transported through their respective layer toward the bipolar junction, where they accumulate and react.[14] In the absence of additional co-ions, H^+ and OH^- accumulate at the BPM junction and recombine (H^+/OH^- recombination; $H^+ + OH^- \rightarrow H_2O$).[12] Forward-bias BPMEAs are of interest for fuel cells,[15−17] redox-flow batteries,[18] and CO_2 reduction.[8,19,20] Therefore, BPMs with low overpotentials under both reverse-bias (driving WD) and forward-bias (driving H^+/OH^- recombination) operation are important.[21]

Adding a catalyst layer at the bipolar junction dramatically lowers overpotentials for the WD reaction and enhances performance in reverse bias.[13,18,22,23] Chen et al. investigated WD-catalyst design principles by correlating the effects of catalyst thickness, site density, and electronic conductivity.[24] However, little is known about the necessity for, or design principles of, catalyst layers during forward-bias operation.[18] Grew et al.[25] derived a trap-assisted recombination mechanism to describe the current densities in H_2-O_2 fuel cells using forward-bias BPMs, but these analyses did not consider the explicit presence of a catalytic layer at the bipolar junction. The presence of a thin graphene oxide layer at the bipolar junction was found to lower overpotentials during both charge (reverse bias; WD) and discharge (forward bias; recombination) in a redox-flow battery.[18] Mechanistic insight into the role of the catalyst layer or design principles for catalytic recombination in BPMs under forward bias remains needed.

Received: September 8, 2022
Accepted: October 17, 2022
Published: October 19, 2022

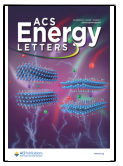

https://doi.org/10.1021/acsenergylett.2c02043
ACS Energy Lett. 2022, 7, 3967−3973

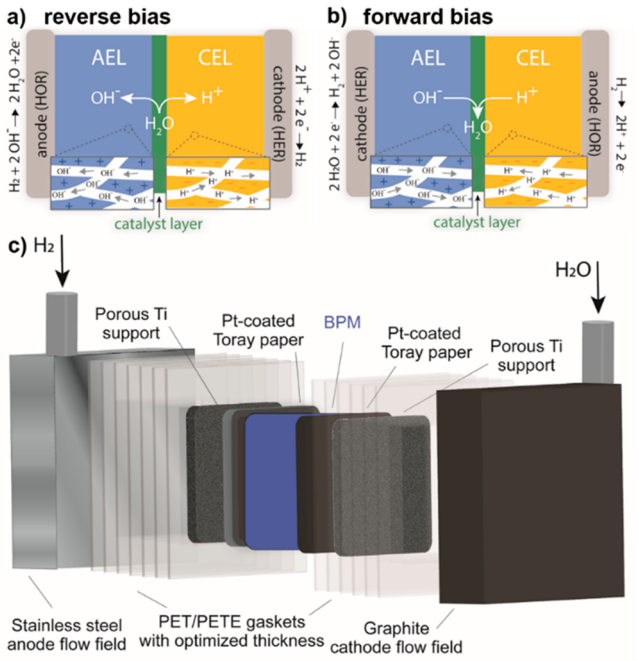

Figure 1. H_2 pump cell schematic. Membrane electrode assembly orientations of (a) reverse- and (b) forward-bias operation. (c) 3D schematic of the hydrogen pump electrochemical cell. Humidified H_2 gas stream is fed to the anode and H_2O to the cathode.

Here, we elucidate the factors that affect recombination by studying the effect of catalyst chemical composition, site density, and electrical conductivity in a BPMEA driving reversible H_2 chemistry at each electrode—i.e., the hydrogen evolution reaction (HER) and hydrogen oxidation reaction (HOR) at the cathode and anode, respectively. We discover that select oxide nanoparticles substantially catalyze the recombination reaction in the bipolar junction under forward bias and find evidence that H^+/OH^- recombination occurs via a surface-initiated mechanism on the oxide catalyst. We show how surface-site density (from BET surface area) and intrinsic catalytic activity dictate the optimal bipolar junction thickness, while the electronic properties of recombination catalysts do not play a significant role, unlike the case of WD, suggesting the lack of a significant electric-field effect on recombination kinetics. Based on experimental data and numerical simulations, we propose a simple rate equation to describe the catalytic H^+/OH^- recombination mechanism and discuss design strategies for recombination catalysts to advance forward-bias BPM technologies.

A H_2-pump electrochemical cell was used to evaluate the BPMs under reverse-bias (WD) and forward-bias (H^+/ OH^- recombination) operation (Figure 1). Humidified H_2 is fed through the anode flow field and deionized (DI) H_2O through the cathode flow field. In reverse bias (Figure 1a), the AEL faces the anode and the CEL faces the cathode. Sufficient reverse bias drives WD at the BPM junction, and H^+/OH^- are transported through their respective ion-exchange layers toward the cathode and anode, respectively. This configuration drives the acidic HER at the cathode and alkaline HOR at the anode. Conversely, forward-bias (Figure 1b) BPMEAs consist of the CEL facing the anode and AEL facing the cathode, yielding opposite pH environments (alkaline HER; acidic HOR). The bipolar junction thus serves as a source or sink for the ionic carriers (H^+ and OH^-) in reverse or forward bias, respectively. We have chosen these electrochemical half-reactions to simplify the cell and promote a systematic study of the H^+/OH^- recombination at the bipolar junction. Alkaline oxygen reduction at the cathode would also suffice and enable direct comparison to BPM H_2-O_2 fuel cells, at the expense of more-complex cell engineering for water transport and cathode stability. As previous reports have focused on accelerating WD using oxide catalysts,[13,24] we investigate whether similar catalytic trends apply to H^+/OH^- recombination in oxide layers at the AEL/CEL interface under forward bias.

Previous work deconvoluted the impedance responses of reverse-bias BPMs and identified two components that could be modeled by an equivalent circuit of a parallel resistor and capacitor (parallel *RC*); one lumped element representing electrode charge-transfer reactions (R_{CT}) and the other representing WD at the bipolar junction (R_{WD}).[24] We used galvanostatic electrochemical impedance spectroscopy (GEIS) to determine the different resistive components of the forward-bias BPMEAs in the H_2-pump cell. Nyquist plots comparing the impedance of pristine BPMs and those containing a catalyst layer (P25-TiO_2, SiO_2) under forward bias are shown in Figure 2, and the fitted data analyses in Tables S1−S3. At open circuit, the Nyquist plots show a primary semicircle (Figure 2a,b). The oxide catalyst layer significantly lowers the resistance comprising the primary semicircle compared to the pristine BPM (<3 $\Omega\cdot cm^2$ vs ~140 $\Omega\cdot cm^2$). Additional semicircles emerge at lower frequencies when current is applied (Figure 2c,d) which are assigned to the anode (acidic HOR) and cathode (basic HER) charge-transfer processes

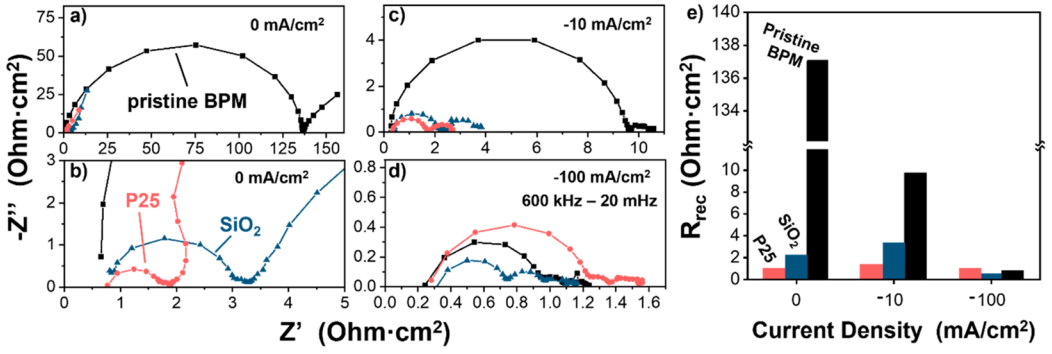

Figure 2. Impedance of forward-bias BPMs. Electrochemical impedance spectroscopy of catalyzed (red: P25-TiO_2, blue: SiO_2) and pristine (black) BPMs from 600 kHz to 20 mHz at (a, b) open-circuit potential (0 mA cm^{-2}), (c) −10 mA cm^{-2}, and (d) −100 mA cm^{-2}. (e) Comparison of the H^+/OH^- recombination resistances, R_{rec}, at different applied currents.

https://doi.org/10.1021/acsenergylett.2c02043
ACS Energy Lett. 2022, 7, 3967−3973

being resolved over the analyzed frequency range (600 kHz–20 mHz). The two lower-frequency *RC* components are similar across all samples (Tables S1–S3) because the anodes, cathodes, and reactions are identical for all cells (in forward bias) and only the BPM junction catalyst is changed. We thus assign the high-frequency *RC* element to H^+/OH^- recombination (kinetic) resistance R_{rec} and elucidate the role of the oxide catalyst layer (Figure 2e). There is initially a large R_{rec} in the pristine BPM, but at sufficient overpotential, R_{rec} is similar between catalyzed and uncatalyzed BPMs. We hypothesize that accumulation of H^+ and OH^- reactants in the BPM junction under large forward biases leads to similar rates of recombination, even in the absence of a catalyst—governed by diffusion of ionic carriers rather than the ion-pair reorganization and recombination.[26]

Galvanostatic polarization curves were collected to assess the H^+/OH^- recombination properties of oxide layers at the AEL | CEL junction (Figure 3), including for P25-TiO_2 as a function

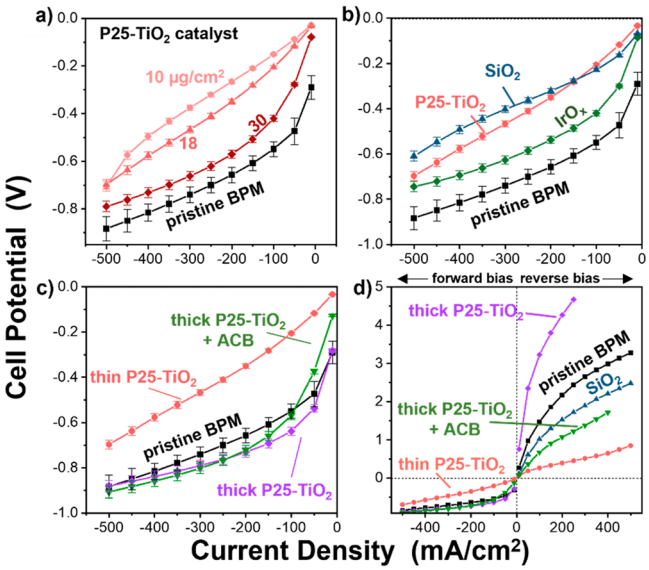

Figure 3. Effect of oxide catalyst layers in forward-bias BPMs. Cell potential as a function of applied current density for different oxide catalyst layers. (a) Loading dependence of P25-TiO_2-catalyzed BPMs under forward bias. Mass loading is estimated according to calibration curves.[24] (b) Effect of catalyst chemical identity in forward-bias BPMs. The optimal loading is plotted for P25-TiO_2, SiO_2, and core/shell Ir/IrO_x. (c) Effect of electrical conductivity on forward-bias BPM performance. Carbon nanoparticles were added to a thick P25-TiO_2 WD catalyst film to enhance conductivity and test the effect on recombination. (d) Full polarization curves of different oxide catalyst layers in the H_2-pump cell (Figure 1). Reverse bias (WD) is defined as positive applied current (to be consistent with previous publications); forward bias is defined as negative current. Error is estimated using the average percent error of oxides with at least two data sets (P25-TiO_2, SiO_2). Error for the pristine BPM is the standard deviation of four samples.

of mass loading/film thickness. Like previous results under reverse bias,[13] we find that oxide nanoparticles lower the cell voltages compared to the pristine BPM. The increased recombination rate is presumably because the poly-protic oxide surfaces mediate recombination of H^+ and OH^- by allowing intermediate proton transfer to/from a large surface area that obviates the need for direct H^+/OH^- recombination in the aqueous phase. For the P25-TiO_2 catalyst layers, thinner films (10 μg cm^{-2} and ~100 nm thick) yielded the best performance. We hypothesize that thinner films lead to lower recombination overpotentials because the rate is dependent on both the number of surface sites (increasing for thick layers) and the concentration of H^+/OH^- (increasing for thin layers). As the weight percent of TiO_2 in the spin-coat ink is increased from 0.1 to 0.5% (~10 to 30 μg cm^{-2}),[24] the cell potentials approach similar values as the pristine BPM, especially at high current densities. To see if performance differences are due to increased particle aggregation at higher spin-coat ink concentrations, we compare the SEM images of catalyst layers formed by 0.1 and 2 wt% P25-TiO_2 (Figure S2) and found that the higher concentration of P25-TiO_2 does not lead to significant particle aggregation.

The above observations demonstrating H^+/OH^- recombination catalysis led us to the question of whether there was a correlation between WD and H^+/OH^- recombination activity. We studied oxide catalysts with varying electronic and WD properties (semiconductor: TiO_2, insulator: SiO_2, and conductor: IrO_x),[13,24] to determine the effects of chemical composition, electrical conductivity, and surface area on catalytic H^+/OH^- recombination. Figure 3b shows the forward-bias polarization curves of BPMs containing the oxide catalyst layers. The optimal loading was investigated for each oxide by adjusting the oxide nanoparticle concentration in the spin-coat inks from 0.1 to 2 wt% (Figure S3). All three oxides catalyze recombination, leading to lower cell voltages compared to the pristine BPM. The effects are especially pronounced below 100 mA cm^{-2}. Interestingly, SiO_2 catalyst layers perform similarly under forward bias to P25-TiO_2 catalyst layers. These results highlight differences in the catalytic processes under reverse (WD) and forward (recombination) biases since the poor WD activity of (electronically insulating) SiO_2 catalysts films does not apparently translate to poor recombination activity under forward bias. SiO_2 WD catalysts in a H_2O BPMEA electrolyzer exhibit much higher cell potentials (>3.5 V at 450 mA cm^{-2}) than P25-TiO_2 (~2 V at 450 mA cm^{-2}).[24] This finding demonstrates that the materials design strategies for WD catalysts do not directly apply to recombination catalysts in forward-bias BPMs. The increase in cell potential for SiO_2 films (Figure S3a) at higher applied currents (>300 mA cm^{-2}) may also be due to the increase in SiO_2 solubility at higher pH as the bipolar junction is flooded with OH^- at the AEL| catalyst-layer interface. Thus, we hypothesize that SiO_2 is not an optimal catalyst for forward-bias BPM applications, but further study of the change in performance at higher applied currents and the role of local pH changes is necessary.

We next investigated the effect of electrical conductivity of the recombination catalyst layer by adding conductive carbon nanoparticles to P25-TiO_2. In reverse bias, we concluded that adding conductive carbon nanoparticles to thick TiO_2 catalyst layers led to performance enhancement by focusing the electric fields at the membrane|catalyst interface within the bipolar junction.[24] We performed similar studies by fabricating "thick" films of P25-TiO_2 (~120 μg cm^{-2}) through spray coating and the performance was compared to a thick film with an additional 55% w/w acetylene black (ACB) (Figure 3c). We also compare the performance of pristine ACB catalyst layers to P25-TiO_2 (Figure S4), which confirms the enhanced catalytic nature of the poly-protic metal-oxide surfaces. We did not include the addition of ACB to the thin, optimal P25-TiO_2

https://doi.org/10.1021/acsenergylett.2c02043
ACS Energy Lett. 2022, 7, 3967–3973

films because it was found to have no positive effect under reverse bias.[24] The thick TiO_2 film leads to higher cell voltages than the thin, optimal TiO_2 loading, yielding higher recombination overpotentials than the catalyst-free, pristine BPM. Conductive carbon nanoparticles (ACB) were then added to the spray-coat ink to change the electrical conductivity of the thick TiO_2 catalyst layer. The enhanced electrical conductivity of the electrically disconnected catalyst layer does lead to lower cell voltages compared to the thick TiO_2 film at lower current densities (~125 mV vs ~275 mV at −10 mA cm^{-2}). However, this effect is not as significant as it was in reverse bias (WD),[24] and at higher applied currents, the performance is similar to the thick P25-TiO_2. For BPMs in reverse bias, the effect of electrical conductivity of the WD catalyst films was significant; the addition of 55% w/w conductive carbon nanoparticles lowered the total cell voltages of thick TiO_2 films (~120 μg cm^{-2}) from ~2.8 V to ~2 V at 150 mA cm^{-2}, leading to similar performance as the thin, optimal P25-TiO_2 loading (18 μg cm^{-2}).[24] Enhanced WD activity in bipolar junctions has been associated with electric fields driving dissociation rates of weak electrolytes such as H_2O.[26] However, the reverse reaction (ion recombination) is likely less affected by the presence of electric fields.[26,27] Our results indicate that the electronic conductivity of the catalyst layer plays only a minor role in H^+/OH^- recombination, thus suggesting electric field strength also plays a minor role unlike has been hypothesized in reverse bias.

Reverse-bias BPM MEAs (Figure 1a) were also tested to study differences between WD and H^+/OH^- recombination (Figure 3d). While WD activity depends on the composition and electronic properties of the oxide nanoparticle film (Figure 3d), recombination activity has less variability with different oxide catalysts. These results reveal that oxide catalysts with poor WD activity do not necessarily have poor recombination activity. The limited variability in cell performance under forward bias suggests that the recombination mechanism is less dependent on the surface chemistry of the catalyst particles, possibly due to the kinetically fast nature of recombination compared to WD.

Finally, we investigated whether the catalyst surface area and film morphology might account for the variation in the catalyzed-BPM performance under forward bias. Anatase TiO_2 catalyst layers with different nanoparticle sizes (5-nm vs 100-nm diameter) were studied to test the effect of catalyst surface area with nanoparticles that possess similar surface chemistry. Figure 4a compares the polarization curves of the different catalyzed BPMs tested under forward bias. Both 5-nm and 100-nm diameter TiO_2 catalysts exhibit lower cell voltages than the pristine BPM, and catalyst layers made with smaller, higher-surface-area particles tend to outperform films from larger-diameter nanoparticles. Surface areas (from gas adsorption measurements) of the oxide catalyst particles shows a trend between the surface area and total cell voltage, where increased surface area leads to lower cell voltages (lower recombination overpotentials; Figure 4b). This finding suggests that the oxide layer at the bipolar junction catalyzes H^+/OH^- recombination through a surface-mediated process. However, additional studies with well-controlled catalyst loading/thickness are necessary to directly compare the effects of catalyst surface area along with the many other parameters that appear to modulate recombination and dissociation rates of water in the BPM (e.g., conductivity, dielectric, surface-

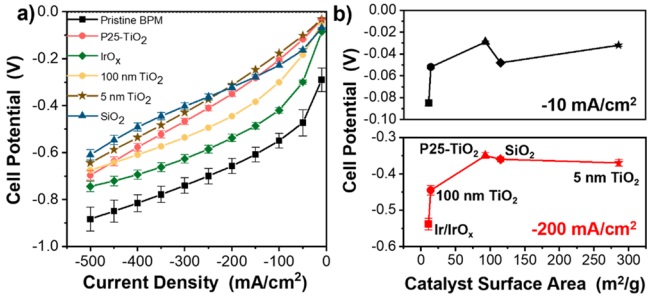

Figure 4. Effect of catalyst surface area in forward-bias BPMs. (a) Forward-bias polarization curves of different catalyzed-BPMEAs. Each oxide layer catalyzes the recombination process and lowers the total cell potential compared to the pristine BPM (black squares). (b) Total cell potential of the MEAs at different applied current densities (top, −10 mA/cm^2; bottom, −200 mA/cm^2) as a function of the BET surface area of the catalyst particles. We present the "optimal" film loading performance of catalyst-ink concentrations varied from 0.1 to 2 wt%. Error is estimated using the average percent error of catalyzed films with at least two data sets (P25-TiO_2 and SiO_2).

hydroxyl concentration, surface area, surface acid/base properties, etc.).

Although there is a general trend with cell performance and catalyst surface area, the similar performance at −200 mA cm^{-2} for BPMs containing SiO_2 (115 m^2 g^{-1}), P25-TiO_2 (93 m^2 g^{-1}), and 5-nm anatase TiO_2 (286 m^2 g^{-1}) catalyst layers suggests there are additional descriptors for H^+/OH^- recombination catalyst activity. We thus investigated the effects of catalyst-layer morphology/thickness. SEM images of the oxide catalyst films spin coated onto the Nafion CEL are shown in Figure 5. The 5-nm anatase TiO_2 particles aggregate

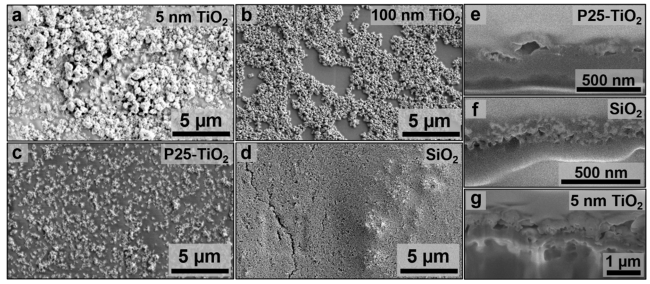

Figure 5. Catalyst-layer film morphology and thickness. Top-down SEM images of (a) 2% 5-nm anatase TiO_2, (b) 2% 100-nm anatase TiO_2, (c) 0.1% P25-TiO_2, and (d) 2% SiO_2. (e–g) Cross-sectional SEM images to estimate catalyst-layer thickness of (e) P25-TiO_2, (f) SiO_2, and (g) 5-nm TiO_2.

and form porous islands but retain uncovered areas of the Nafion® membrane (Figure 5a). The larger, 100-nm anatase particles formed films with less particle stacking and exhibited even larger areas of uncovered CEL (Figure 5b). P25-TiO_2 spin-coated films form homogeneous, thin films with limited particle stacking and enhanced dispersibility compared to 5-nm and 100-nm anatase TiO_2 (Figure 5c). The enhanced dispersibility and film homogeneity likely accounts for the similar performance to the 5-nm anatase, even though P25-TiO_2 has about 3-fold less surface area. Accessible catalyst surface area is likely a better performance descriptor than the BET measurements. SiO_2 forms a homogeneous film with smaller aggregate sizes than the other oxides, leading to

https://doi.org/10.1021/acsenergylett.2c02043
ACS Energy Lett. 2022, 7, 3967−3973

porous, continuous films without a significant proportion of the CEL surface exposed (Figure 5d). SiO_2-catalyst layers are thicker than P25-TiO_2, but the overall cell performance and R_{rec} is similar. Figure 5e−g shows cross-sectional SEM images of the catalyst layers coated on the CEL. The optimal loading of P25-TiO_2 has a film thickness of ∼100 nm, SiO_2 ∼230 nm, and 5-nm TiO_2 ∼1 μm. We thus find that recombination catalyst layers of different oxides have varying thicknesses/morphologies which lead to similar rates of reaction.

The above data led us to use simple numerical simulations of the bipolar junction to help elucidate design criteria for recombination catalyst layers. Figure 6 shows the current

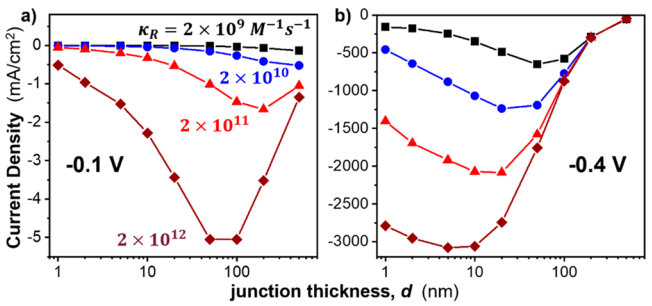

Figure 6. Simulated current densities in forward-bias BPMs. Numerical simulations of current density as a function of bipolar junction thickness (d) for BPMs with varying rates of recombination (k_R) at forward-bias overpotentials of (a) −0.1 V and (b) −0.4 V. As both the driving force (applied potential) and rate reaction (k_R) increase, the optimal junction thickness decreases.

density as a function of bipolar-junction thickness (d) for different recombination rate constants (k_R) and applied potentials. As k_R increases, the simulated curves show the optimal junction thickness (d_{opt}) is lowered, and the overall rate of recombination (current density) is enhanced. Additionally, the parabolic-like shape of the simulated loading-dependent performance (Figure 6a) indicates that catalyst layers with different rate constants and junction thicknesses can lead to similar current densities, consistent with experiment. Our experimental results reveal higher current densities (∼50 mA cm^{-2}) than expected for an uncatalyzed reaction (k_R ≈ 10^{11} M^{-1} s^{-1}; <10 mA cm^{-2}) at low applied bias (−0.1 V; Figure 6a), corroborating the catalytic nature of the metal oxides at low overpotentials (Figure 3). At higher overpotentials (−0.4 V; Figure 6b), simulations show higher current densities than experimentally observed for small junction thicknesses (<100 nm), but the parabolic nature of the simulated $J-V$ curves confirm that the junction thicknesses we experimentally probe here (≥100 nm) yield similar current densities (<500 mA cm^{-2}).

These simulations suggest that the higher current densities may only be achieved with thin catalyst layers (<100 nm). We hypothesize that if the rate of recombination is sufficiently fast, a smaller bipolar junction will lower transport limitations, increasing H^+/OH^- collisions and thus rates of recombination. Conversely, if the rate of recombination is slower on the catalyst surface, a thicker junction is necessary to accommodate more injected H^+ and OH^- charge carriers while maintaining concentrations closer to their equilibrium values. Since we expect SiO_2 to exhibit lower k_R values (see below), this provides a possible explanation for the observed differences between P25-TiO_2 and SiO_2 catalyst layers under forward bias; the optimal P25-TiO_2 film is a thin layer with sparse coverage and SiO_2 performs best with thicker films that maintain porosity.

We showed previously that P25-TiO_2 has much better WD performance under reverse bias and thus higher WD rate constants than SiO_2.[24] Since WD (k_D) and H^+/OH^- recombination (k_R) rate constants are related by the water auto-dissociation constant K_w (eq 1, with appropriate units), P25-TiO_2 would be expected to also have higher rates of recombination and thus lower d_{opt} than SiO_2, in line with our experimental observations.

$$K_w = \frac{k_D}{k_R} \tag{1}$$

Polarization curves of catalyzed BPMs with controlled catalyst loading corroborate these hypotheses (Figure S4). In addition to the effects of recombination rate, comparing performance of anatase- and P25-TiO_2 suggests an effect of catalytic-site density. While 5-nm diameter anatase TiO_2 has higher surface area than P25-TiO_2, the enhanced catalytic-site density is compensated by worse film coverage and larger bipolar junction thicknesses. This illustrates the importance of both accessible catalyst surface area and bipolar junction thickness when considering criteria for designing H^+/OH^- recombination catalyst layers.

The above experimental and simulation data led us to consider simple rate equations for the catalyzed and uncatalyzed H^+/OH^- recombination mechanisms. For uncatalyzed recombination, the reaction can be written as the microscopic reverse of WD:

$$H^+ + OH^- \leftrightarrow H_2O \tag{2}$$

The recombination rate is the product of the H^+ and OH^- concentrations with a rate constant, k_R:

$$\text{Rate} = k_R[H^+][OH^-] \tag{3}$$

where k_R is typically related to the auto-dissociation of pure H_2O (K_w) by eq 1, and has values on the order of ∼10^{11} M^{-1} s^{-1} in liquid H_2O at 25 °C.[28,29]

For surface-mediated recombination, the oxide catalyst may participate in similar acid/base proton-transfer mechanisms hypothesized by Simons to explain WD catalysis at the AEL/CEL interface.[30] As protons are injected into the bipolar junction, they adsorb onto active metal-oxide catalyst sites (MO*) to form protonated intermediates (eq 4), where the active site can be a terminal- or bridging-surface oxygen possessing a range of apparent pK_a values.[31] Similarly, injected hydroxides diffuse to the bipolar junction where the surface-mediated recombination produces free H_2O (eq 5).

$$H^+ + MO^* \overset{k'_{cat}}{\leftrightarrow} MOH^+ \tag{4}$$

$$OH^- + MOH^+ \overset{k''_{cat}}{\leftrightarrow} H_2O + MO^* \tag{5}$$

We write the forward rate equations (r_{fwd}) according to the surface-mediated mechanisms (eqs 4 and 5) to describe the rate of recombination in the bipolar junction under forward bias at steady state where the rate of both steps must be equal (ignoring the backward reactions as the system is far from equilibrium):

$$r_{fwd} = k'_{cat}[H^+][MO^*] = k''_{cat}[OH^-][MOH^+] \tag{6}$$

https://doi.org/10.1021/acsenergylett.2c02043
ACS Energy Lett. 2022, 7, 3967−3973

The catalytic rate constants (k'_{cat}, k''_{cat}) thus provide structure−property relationships intrinsic to the catalyst layer. We note that in some cases the backward dissociation rate constants may need to be considered due to the varying proton affinities of surface oxygen groups and the expected pH gradient across the catalyst layer within the bipolar junction. However, while additional studies are necessary to validate/revise the model and systematically determine factors affecting the intrinsic rate constants, the generalized rate equation can aid in designing recombination catalyst layers. As the catalyst-layer thickness (d) increases, the average concentrations of H^+/OH^- will decrease, but the number of active MO* sites over which recombination can occur will increase. These two competing factors appear to lead to an optimal junction thickness based on the intrinsic catalytic rate constants (k'_{cat}, k''_{cat}) and catalyst surface area, qualitatively consistent with our experimental and simulated results.

In sum, we showed that oxide films lower recombination overpotentials compared to the pristine BPM through surface-mediated H^+/OH^- recombination. Benchmarking these results with commercial BPMs is important for distinguishing impacts to the field. However, we have found it difficult to integrate commercial BPMs into an MEA and they possess poor performance, not representative of the actual BPM, due to the mechanical reinforcement yielding ribs in the membrane. While the effects of a catalyst layer have not been previously studied in similar H_2-pump electrochemical cell configurations with these exact AEL, CEL, and catalyst-layer compositions, we find that the R_{rec} values for the catalyzed BPMs reported here (<2.5 $\Omega\cdot cm^2$) are lower than values reported in an aqueous redox flow battery (~7.5 $\Omega\cdot cm^2$ at 2 mA cm^{-2})[18] as well as various commercially available BPMs studied in acid/base flow batteries (~30−2.5 $\Omega\cdot cm^2$).[32] Our experimental and simulated data suggests that the optimal catalyst-layer/junction thickness is dictated by the intrinsic rate constants and accessible catalyst surface area. However, these are complex systems with many other parameters that can modulate recombination and dissociation rates of water in the BPM (e.g., conductivity, dielectric constant, surface hydroxyl concentration, morphology, surface acid/base properties, etc.). Further controlling the catalyst-layer deposition to systematically test film thickness and surface area/loading dependence will aid in determining the various factors affecting the intrinsic recombination rate constants, guiding future materials design strategies. Additionally, controlling the concentration of surface oxygen groups could be a useful way to correlate catalytic sites in WD/recombination catalyst layers. Tuning the catalyst-layer activity, thickness, and accessible surface area will minimize WD/recombination overpotentials, enabling the design of catalyst layers for the desired electrochemical response. Thin catalyst layers with high intrinsic WD/recombination rate constants are likely advantageous in applications that require low overpotentials in both forward and reverse biases such as batteries,[18,32] while catalysts that possess low WD activity such as thick, electrically insulative catalyst films may be used analogously to rectify semiconductor *pn* junctions for protonic[33] and electrochromic[34] diodes. Modifying these design strategies and engineering the catalyst layer for particular applications, and ionic recombination processes will provide a better understanding of the potential for BPMs to advance electrochemical technologies in energy storage/conversion, separations, chemical synthesis, and carbon capture/utilization.

■ ASSOCIATED CONTENT

Supporting Information

The Supporting Information is available free of charge at https://pubs.acs.org/doi/10.1021/acsenergylett.2c02043.

Polarization curves of a pristine BPM with DI H_2O and N_2-purged DI H_2O fed to the cathode, SEM images of "thin" and "thick" P25-TiO_2 catalyst layers, loading dependence of catalyzed BPMs, tables of impedance values derived from GEIS experiments, polarization curves of P25-TiO_2, SiO_2, and ACB with controlled catalyst loadings, and experimental methods (PDF)

■ AUTHOR INFORMATION

Corresponding Author

Shannon W. Boettcher − *Department of Chemistry and Biochemistry and the Oregon Center for Electrochemistry, University of Oregon, Eugene, Oregon 97403, United States;* orcid.org/0000-0001-8971-9123; Email: swb@uoregon.edu

Authors

James B. Mitchell − *Department of Chemistry and Biochemistry and the Oregon Center for Electrochemistry, University of Oregon, Eugene, Oregon 97403, United States*

Lihaokun Chen − *Department of Chemistry and Biochemistry and the Oregon Center for Electrochemistry, University of Oregon, Eugene, Oregon 97403, United States*

Kurt Langworthy − *Center for Advanced Materials Characterization in Oregon, University of Oregon, Eugene, Oregon 97403, United States*

Kevin Fabrizio − *Department of Chemistry and Biochemistry and the Oregon Center for Electrochemistry, University of Oregon, Eugene, Oregon 97403, United States;* orcid.org/0000-0001-9700-1824

Complete contact information is available at: https://pubs.acs.org/10.1021/acsenergylett.2c02043

Notes

The authors declare the following competing financial interest(s): The authors have submitted a provisional patent on the topic of this manuscript.

■ ACKNOWLEDGMENTS

This work was supported by the U.S. Office of Naval Research, grant N00014-20-1-2517 (to S.W.B.). We acknowledge the use of shared instrumentation in the Center for Advanced Materials Characterization in Oregon (CAMCOR) and the Phil and Penny Knight Campus for Accelerating Scientific Impact. We also acknowledge key discussions with Shane Ardo on dissociation and recombination mechanisms in BPMs.

■ REFERENCES

(1) Pärnamäe, R.; Mareev, S.; Nikonenko, V.; Melnikov, S.; Sheldeshov, N.; Zabolotskii, V.; Hamelers, H. V. M.; Tedesco, M. Bipolar Membranes: A Review on Principles, Latest Developments, and Applications. *J. Membr. Sci.* **2021**, *617*, 118538.

(2) Luo, T.; Abdu, S.; Wessling, M. Selectivity of Ion Exchange Membranes: A Review. *J. Membr. Sci.* **2018**, *555*, 429−454.

(3) Giesbrecht, P. K.; Freund, M. S. Recent Advances in Bipolar Membrane Design and Applications. *Chem. Mater.* **2020**, *32* (19), 8060−8090.

(4) Pourcelly, G. Electrodialysis with Bipolar Membranes: Principles, Optimization, and Applications. *Russ. J. Electrochem.* **2002**, *38* (8), 919−926.
(5) Fernandez-Gonzalez, C.; Dominguez-Ramos, A.; Ibañez, R.; Irabien, A. Electrodialysis with Bipolar Membranes for Valorization of Brines. *Sep. Purif. Rev.* **2016**, *45* (4), 275−287.
(6) Balster, J.; Stamatialis, D. F.; Wessling, M. Electro-Catalytic Membrane Reactors and the Development of Bipolar Membrane Technology. *Chem. Eng. Process.: Process Intensif.* **2004**, *43* (9), 1115−1127.
(7) Blommaert, M. A.; Verdonk, J. A. H.; Blommaert, H. C. B.; Smith, W. A.; Vermaas, D. A. Reduced Ion Crossover in Bipolar Membrane Electrolysis via Increased Current Density, Molecular Size, and Valence. *ACS Appl. Energy Mater.* **2020**, *3* (6), 5804−5812.
(8) Li, Y. C.; Yan, Z.; Hitt, J.; Wycisk, R.; Pintauro, P. N.; Mallouk, T. E. Bipolar Membranes Inhibit Product Crossover in CO2 Electrolysis Cells. *Adv. Sustainable Syst.* **2018**, *2* (4), 1700187.
(9) Oener, S. Z.; Twight, L. P.; Lindquist, G. A.; Boettcher, S. W. Thin Cation-Exchange Layers Enable High-Current-Density Bipolar Membrane Electrolyzers via Improved Water Transport. *ACS Energy Lett.* **2021**, *6* (1), 1−8.
(10) Mayerhöfer, B.; McLaughlin, D.; Böhm, T.; Hegelheimer, M.; Seeberger, D.; Thiele, S. Bipolar Membrane Electrode Assemblies for Water Electrolysis. *ACS Appl. Energy Mater.* **2020**, *3* (10), 9635−9644.
(11) Vermaas, D. A.; Smith, W. A. Synergistic Electrochemical CO2 Reduction and Water Oxidation with a Bipolar Membrane. *ACS Energy Lett.* **2016**, *1* (6), 1143−1148.
(12) Pärnamäe, R.; Mareev, S.; Nikonenko, V.; Melnikov, S.; Sheldeshov, N.; Zabolotskii, V.; Hamelers, H. V. M.; Tedesco, M. Bipolar Membranes: A Review on Principles, Latest Developments, and Applications. *J. Membr. Sci.* **2021**, *617*, 118538.
(13) Oener, S. Z.; Foster, M. J.; Boettcher, S. W. Accelerating Water Dissociation in Bipolar Membranes and for Electrocatalysis. *Science* **2020**, *369* (6507), 1099−1103.
(14) Tufa, R. A.; Blommaert, M. A.; Chanda, D.; Li, Q.; Vermaas, D. A.; Aili, D. Bipolar Membrane and Interface Materials for Electrochemical Energy Systems. *ACS Appl. Energy Mater.* **2021**, *4* (8), 7419−7439.
(15) Ünlü, M.; Zhou, J.; Kohl, P. A. Hybrid Anion and Proton Exchange Membrane Fuel Cells. *J. Phys. Chem. C* **2009**, *113* (26), 11416−11423.
(16) Ahlfield, J. M.; Liu, L.; Kohl, P. A. PEM/AEM Junction Design for Bipolar Membrane Fuel Cells. *J. Electrochem. Soc.* **2017**, *164* (12), F1165.
(17) Lobyntseva, E.; Kallio, T.; Kontturi, K. Bipolar Membranes in Forward Bias Region for Fuel Cell Reactors. *Electrochim. Acta* **2006**, *51* (7), 1165−1171.
(18) Yan, Z.; Wycisk, R. J.; Metlay, A. S.; Xiao, L.; Yoon, Y.; Pintauro, P. N.; Mallouk, T. E. High-Voltage Aqueous Redox Flow Batteries Enabled by Catalyzed Water Dissociation and Acid-Base Neutralization in Bipolar Membranes. *ACS Cent. Sci.* **2021**, *7* (6), 1028−1035.
(19) Pătru, A.; Binninger, T.; Pribyl, B.; Schmidt, T. J. Design Principles of Bipolar Electrochemical Co-Electrolysis Cells for Efficient Reduction of Carbon Dioxide from Gas Phase at Low Temperature. *J. Electrochem. Soc.* **2019**, *166* (2), F34−F43.
(20) Pribyl-Kranewitter, B.; Beard, A.; Schuler, T.; Diklić, N.; Schmidt, T. J. Investigation and Optimisation of Operating Conditions for Low-Temperature CO2 Reduction to CO in a Forward-Bias Bipolar-Membrane Electrolyser. *J. Electrochem. Soc.* **2021**, *168* (4), 043506.
(21) Yan, Z.; Mallouk, T. E. Bipolar Membranes for Ion Management in (Photo) Electrochemical Energy Conversion. *Acc. Mater. Res.* **2021**, *2* (12), 1156−1166.
(22) Shehzad, M. A.; Yasmin, A.; Ge, X.; Ge, Z.; Zhang, K.; Liang, X.; Zhang, J.; Li, G.; Xiao, X.; Jiang, B.; Wu, L.; Xu, T. Shielded Goethite Catalyst That Enables Fast Water Dissociation in Bipolar Membranes. *Nat. Commun.* **2021**, *12* (1), 9.
(23) Manohar, M.; Das, A. K.; Shahi, V. K. Efficient Bipolar Membrane with Functionalized Graphene Oxide Interfacial Layer for Water Splitting and Converting Salt into Acid/Base by Electrodialysis. *Ind. Eng. Chem. Res.* **2018**, *57* (4), 1129−1136.
(24) Chen, L.; Xu, Q.; Oener, S. Z.; Fabrizio, K.; Boettcher, S. W. Design Principles for Water Dissociation Catalysts in High-Performance Bipolar Membranes. *Nat. Commun.* **2022**, *13*, 3846.
(25) Grew, K. N.; McClure, J. P.; Chu, D.; Kohl, P. A.; Ahlfield, J. M. Understanding Transport at the Acid-Alkaline Interface of Bipolar Membranes. *J. Electrochem. Soc.* **2016**, *163* (14), F1572.
(26) Onsager, L. Deviations from Ohm's Law in Weak Electrolytes. *J. Chem. Phys.* **1934**, *2* (9), 599−615.
(27) Langevin, P. Recombinaison et Mobilites Des Ions Dans Les Gaz. *Ann. Chim. Phys.* **1903**, *28* (433), 122.
(28) Eigen, M.; De Maeyer, L. Untersuchungen über die Kinetik der Neutralisation. I. *Z. Elektrochem., Ber. Z. Elektrochem., Ber. Bunsenges. Phys. Chem.* **1955**, *59* (10), 986−993.
(29) Natzle, W. C.; Moore, C. B. Recombination of Hydrogen Ion (H+) and Hydroxide in Pure Liquid Water. *J. Phys. Chem.* **1985**, *89* (12), 2605−2612.
(30) Simons, R. Strong Electric Field Effects on Proton Transfer between Membrane-Bound Amines and Water. *Nature* **1979**, *280* (5725), 824−826.
(31) Bunker, B. C.; Casey, W. H.*The Aqueous Chemistry of Oxides*; Oxford University Press: New York, 2016; pp 132−162.
(32) Al-Dhubhani, E.; Pärnamäe, R.; Post, J. W.; Saakes, M.; Tedesco, M. Performance of Five Commercial Bipolar Membranes under Forward and Reverse Bias Conditions for Acid-Base Flow Battery Applications. *J. Membr. Sci.* **2021**, *640*, 119748.
(33) Schulte, L.; White, W.; Renna, L. A.; Ardo, S. Turning Water into a Protonic Diode and Solar Cell via Doping and Dye Sensitization. *Joule* **2021**, *5* (9), 2380−2394.
(34) Malti, A.; Gabrielsson, E. O.; Crispin, X.; Berggren, M. An Electrochromic Bipolar Membrane Diode. *Adv. Mater.* **2015**, *27* (26), 3909−3914.

https://doi.org/10.1021/acsenergylett.2c02043
ACS Energy Lett. 2022, 7, 3967−3973